Title

Translational profiling identifies a cascade of damage initiated in motor neurons and spreading to glia in mutant SOD1-mediated ALS

Journal

Proceedings of the National Academy of Sciences of the United States of America, 112(50)

ISSN

0027-8424

Authors

Sun, Shuying
Sun, Ying
Ling, Shuo-Chien
et al.

Publication Date

2015-12-15

DOI

10.1073/pnas.1520639112

Peer reviewed

Translational profiling identifies a cascade of damage initiated in motor neurons and spreading to glia in mutant SOD1-mediated ALS

Shuying Sun[a,b], Ying Sun[a,b], Shuo-Chien Ling[a,b,1], Laura Ferraiuolo[c,2], Melissa McAlonis-Downes[a,b], Yiyang Zou[b], Kevin Drenner[a,b], Yin Wang[a,b], Dara Ditsworth[a,b], Seiya Tokunaga[a,b], Alex Kopelevich[b], Brian K. Kaspar[c], Clotilde Lagier-Tourenne[a,d,3], and Don W. Cleveland[a,b,d,4]

[a]Ludwig Institute for Cancer Research, University of California at San Diego, La Jolla, CA 92093; [b]Department of Cellular and Molecular Medicine, University of California at San Diego, La Jolla, CA 92093; [c]The Research Institute at Nationwide Children's Hospital, Department of Neuroscience, The Ohio State University, Columbus, OH 43205; and [d]Department of Neurosciences, University of California at San Diego, La Jolla, CA 92093

Contributed by Don W. Cleveland, October 26, 2015 (sent for review September 24, 2015)

Ubiquitous expression of amyotrophic lateral sclerosis (ALS)-causing mutations in superoxide dismutase 1 (SOD1) provokes noncell autonomous paralytic disease. By combining ribosome affinity purification and high-throughput sequencing, a cascade of mutant SOD1-dependent, cell type-specific changes are now identified. Initial mutant-dependent damage is restricted to motor neurons and includes synapse and metabolic abnormalities, endoplasmic reticulum (ER) stress, and selective activation of the PRKR-like ER kinase (PERK) arm of the unfolded protein response. PERK activation correlates with what we identify as a naturally low level of ER chaperones in motor neurons. Early changes in astrocytes occur in genes that are involved in inflammation and metabolism and are targets of the peroxisome proliferator-activated receptor and liver X receptor transcription factors. Dysregulation of myelination and lipid signaling pathways and activation of ETS transcription factors occur in oligodendrocytes only after disease initiation. Thus, pathogenesis involves a temporal cascade of cell type-selective damage initiating in motor neurons, with subsequent damage within glia driving disease propagation.

ALS | SOD1 | cell type selective toxicity | bacTRAP | RNA profiling

Amyotrophic lateral sclerosis (ALS) is an adult-onset neurodegenerative disease with loss of upper and lower motor neurons that leads to fatal paralysis, with a typical disease course of 1–5 y (1). Dominant mutations in the Cu/Zn superoxide dismutase (SOD1) gene (2) account for 20% of familial ALS. Analysis of chimeric mice comprised of mixtures of wild type and mutant-expressing cells (3, 4) and use of cell type-selective excision of ubiquitously expressed SOD1 mutant transgenes (5–9) have established that disease pathogenesis is noncell autonomous, a mechanistic feature that is likely to be common to many neurological disorders (10). Mutant SOD1 in motor neurons accelerates disease onset, but does not affect the rate of disease progression (5, 7, 8). Mutant synthesis by neighboring glial cells, especially astrocytes (8) and microglia (5), has been shown to accelerate disease progression (5, 8). Mutant SOD1 gene inactivation in $NG2^+$ oligodendrocyte progenitors, but not in already matured oligodendroctyes, of adult mice has been reported to delay the age of disease onset (11). Mutant synthesis in as-yet unidentified cell types beyond motor neurons and oligodendrocytes also drives the onset of disease in ALS mice, as demonstrated by delayed initiation of disease in mice in which all motor neurons and oligodendrocytes are mutant-expressing but variable proportions of other cell types express mutant SOD1 (4).

Two key questions in understanding the pathogenic mechanisms of ALS are what causes the selective degeneration of motor neurons from a widely expressed mutant gene and what genetic regulators of aging influence late-onset disease. Multiple pathways for toxicity of mutant SOD1 have been implicated, including misfolded protein triggering abnormal mitochondrial function, endoplasmic reticulum (ER) stress, axonal transport defects, excessive production of extracellular superoxide, and oxidative damage from aberrantly secreted mutant SOD1 (reviewed in ref. 12). What damage occurring during the course of disease is accumulated within motor neurons, astrocytes, or oligodendrocytes remains unknown, however.

Previous attempts to analyze gene expression changes caused by mutant SOD1 within defined cell populations in the central nervous system (CNS) have relied on the physical enrichment of target cell populations, with either laser-capture microdissection (13–17) or fluorescence-activated cell sorting (18). These approaches have clear disadvantages, however, including cross-contamination from neighboring cells/environments; isolation of RNAs only from neuronal cell bodies but not dendrites, axons, or synapses; and artifacts introduced during cellular isolation procedures. In addition, becaue of technical limitations, most

Significance

Amyotrophic lateral sclerosis can be caused by a mutation in superoxide dismutase. Ubiquitously expressed, disease mechanism involves damage within motor neurons (whose degeneration is responsible for progressive paralysis) and glia. By combining ribosome affinity purification from each of three cell types, a temporal cascade of damage is identified that initiates within motor neurons, with subsequent damage within glia driving disease propagation. Mutant-dependent damage to motor neurons, which are shown to express very low levels of endoplasmic reticulum chaperones, includes synapse and metabolic abnormalities and selective activation of the PERK arm of the unfolded protein response. Early changes in astrocytes are to genes involved in inflammation and metabolism, while dysregulation of myelination and lipid signaling pathways in oligodendrocytes occurs only after disease initiation.

Author contributions: S.S. and D.W.C. designed research; S.S., S.-C.L., L.F., M.M.-D., Y.Z., K.D., Y.W., D.D., S.T., and A.K. performed research; B.K.K. and C.L.-T. contributed new reagents/analytic tools; S.S. and Y.S. analyzed data; and S.S. and D.W.C. wrote the paper.

The authors declare no conflict of interest.

Freely available online through the PNAS open access option.

Data deposition: The raw RNA-seq data have been deposited in the Gene Expression Omnibus (GEO) database, www.ncbi.nlm.nih.gov/geo (accession no. GSE74724).

[1]Present address: Department of Physiology, National University of Singapore, Singapore 117549.

[2]Present address: Sheffield Institute for Translational Neuroscience, University of Sheffield, Sheffield S10 2TN, United Kingdom.

[3]Present address: MassGeneral Institute for Neurodegenerative Diseases, Department of Neurology, Massachusetts General Hospital, Charlestown, MA 02129.

[4]To whom correspondence should be addressed. Email: dcleveland@ucsd.edu.

This article contains supporting information online at www.pnas.org/lookup/suppl/doi:10.1073/pnas.1520639112/-/DCSupplemental.

previous studies have focused on motor neurons alone or a mixture of cells from white matter rather than on individual glial cell types. Furthermore, most previous work used transgenic mice with a highly accelerated disease course from a very high degree of overexpression of mutant SOD1, which in the most frequently studied mouse (19) yields >20 times the normal endogenous level by end-stage disease, raising concern about how closely the mechanism of toxicity in this accelerated model reflects the human situation.

Non–cell-autonomous toxicity has been demonstrated in cell cultures as well, with astrocytes (20–25) or microglia (26) carrying SOD1 mutations generating toxicity to cocultured embryonic motor neurons. Although gene expression changes induced by the $SOD1^{G93A}$ mutant in such cocultures have been reported (27), the extent to which this reflects age-dependent disease course has not been established.

Here we coupled high-throughput RNA sequencing with the translating ribosome affinity purification (TRAP) methodology (28, 29) to evaluate damage within motor neurons, astrocytes, and oligodendrocytes during the course of disease in mice that develop fatal ALS-like paralysis from ubiquitous expression of a moderate level of the familial ALS-causing mutation $SOD1^{G37R}$ (5). BacTRAP reporter transgenes that encode an EGFP-tagged ribosomal protein L10a (Rpl10a) and driven by a cell type-specific transgene promoter allow isolation of actively translating, polyribosome-associated mRNAs from specific cell types in the CNS. Ribosome subunits and the bound mRNAs can be maintained intact and isolated by EGFP immunoprecipitation from an unstressed, in vivo cellular environment with intact cell–cell connections at any chosen time point during aging. With this approach, we have identified a cascade of damage, including selective activation of the protein kinase RNA-like endoplasmic reticulum kinase or PRKR-like ER kinase (PERK) arm of the unfolded protein response (UPR), to start within motor neurons, followed by dysregulation of metabolic and inflammatory genes in astrocytes and membrane proteins and lipid signaling pathways in oligodendrocytes.

Results

Isolation of Translated mRNAs from Motor Neurons, Astrocytes, or Oligodendrocytes. To determine the damage caused by ALS-linked mutant SOD1 within spinal motor neurons, astrocytes, or oligodendrocytes during the disease course, we mated a mouse line (*LoxSOD1*^{G37R}) that develops age-dependent, fatal paralytic motor neuron disease from ubiquitous expression of a moderate level of an ALS-linked point mutation in SOD1 (5) to bacTRAP reporter mouse lines (28, 29) (Fig. 1*A*). The *LoxSOD1*^{G37R} line was chosen because of its wide use in identifying cell types whose mutant SOD1 synthesis contributes to a non–cell-autonomous disease mechanism (5, 8, 11, 30, 31) and in which overt disease onset initiates at approximately 8 mo of age (Fig. 1*B*). The disease course after initiation includes nearly complete denervation-induced muscle atrophy and accompanying weight loss, motor neuron death, and progressive paralysis (5).

Cohorts of *LoxSOD1*^{G37R} mice expressing EGFP-tagged ribosome protein Rpl10a only within motor neurons (*Chat*-bacTRAP), astrocytes (*Aldh1l1*-bacTRAP), or oligodendrocytes (*Cnp1*-bacTRAP) were obtained (28, 29) (Fig. 1*A*). All mice were in a common C57BL/6 genetic background. The predicted EGFP-Rpl10a expression patterns in spinal cords of the three reporter mouse lines were confirmed by immunofluorescence (Fig. 1*C*). *Chat* promoter-driven EGFP-Rpl10a was expressed in the same cell

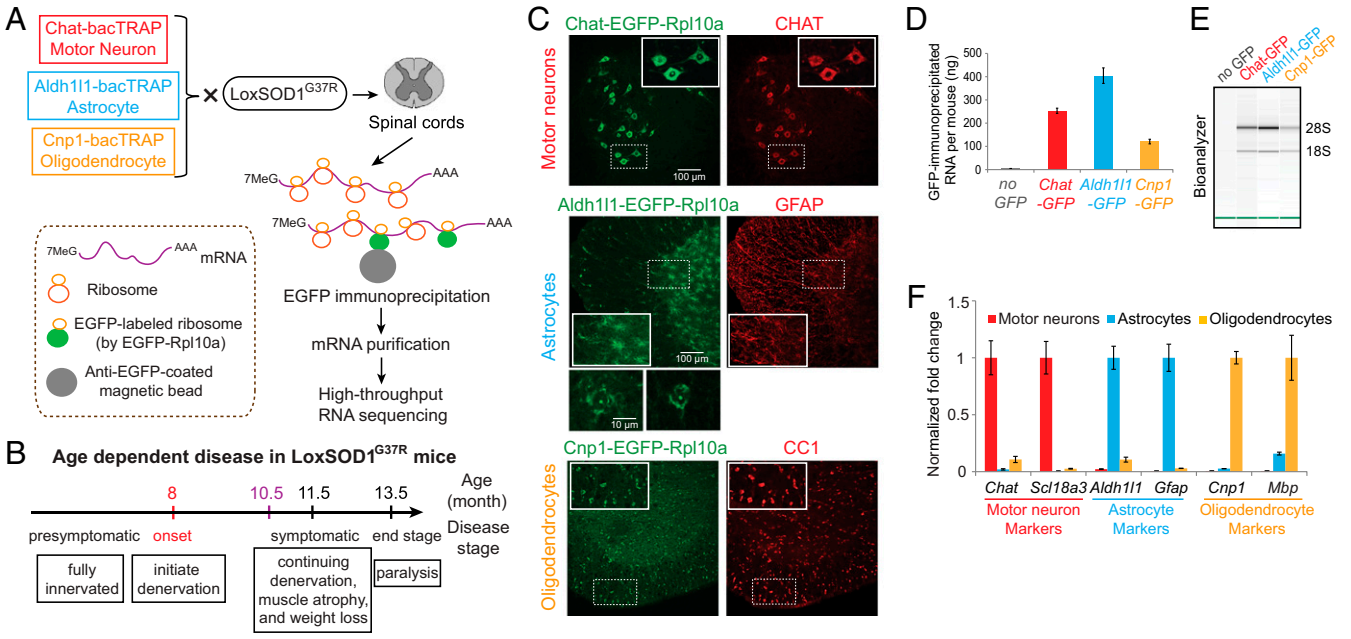

Fig. 1. The bacTRAP methodology for isolating cell type-specific translational mRNAs. (*A*) The experimental design to identify cell type-specific damages in motor neurons, astrocytes, and oligodendrocytes caused by the $SOD1^{G37R}$ mutant, coupling the bacTRAP methodology and high-throughput RNA sequencing. The polyribosome-associated translational mRNAs were isolated by EGFP immunoprecipitation from specifically labeled cell types in the spinal cord of bacTRAP reporter mice. (*B*) The disease course of the $SOD1^{G37R}$ transgenic mouse. To identify early changes, RNA from all three cell types was first isolated at disease onset (~8 mo; red). RNA from oligodendrocytes was also examined at an early symptomatic stage (~10.5 mo; purple). (*C*) Direct fluorescence of GFP (for motor neuron reporter) or double immunostaining of mouse spinal cord with an anti-GFP antibody (green, for astrocyte and oligodendrocyte reporters) and antibodies for motor neuron marker Chat (red), astrocyte marker GFAP (red), and marker for oligodendrocytes CC1 (red). (*D*) Average amount of GFP-immunoprecipitated RNA from each spinal cord of the three EGFP-Rpl10a reporter mice and mice without the GFP transgene. (*E*) The quality of RNA after immunoprecipitation was measured with a Bioanalyzer. The intact 18S and 28S bands demonstrate that the RNA was not degraded. (*F*) qRT-PCR for motor neuron markers *Chat* and *Slcl18a3*(VAChT), astrocyte markers *Aldh1* and *Gfap*, and oligodendrocyte markers *Cnp1* and *Mbp*.

population that expressed the motor neuron-specific protein choline acetyltransferase (Chat). The *Aldh1l1* promoter-driven EGFP-tagged ribosome-labeled cells exhibited the morphology expected for astrocytes with many fine processes (32, 33) that partially overlap the astrocyte marker GFAP, whose localization is restricted to a subset of astrocytic cytoplasm (33). The *Cnp1* promoter-driven EGFP-RPl10a was specifically expressed in oligodendrocytes, as indicated by coaccumulation with CC1. In all three cases, EGFP-tagged Rpl10a was found diffusely within the corresponding cytoplasm and bound to nucleoli (Fig. 1*C*), as expected for a ribosomal protein.

To identify early changes that might trigger or contribute directly to pathogenesis rather than reflect consequences of initial motor neuron degeneration and death, we harvested spinal cords from each of the three EGFP-Rpl10a mouse lines, with or without the *LoxSOD1*^{G37R} transgene, from 8-mo-old mice, an age at which muscle denervation in most mutant animals had started but before overt phenotypic symptoms had developed (30) (Fig. 1*B*). GFP immunoprecipitation of extracts from mouse spinal cords successfully recovered polyribosome-associated mRNAs from each EGFP-Rpl10a reporter mouse, with very little background RNA from mice without the GFP-containing transgene (Fig. 1*D*). mRNAs purified by EGFP immunoprecipitation from motor neurons, astrocytes, and oligodendrocytes remained intact (Fig. 1*E*) and were highly enriched for corresponding marker genes, including *Chat* and *Slc18a3* (VAChT) for motor neurons, *Aldh1l1* and *Gfap* for astrocytes, and *Cnp1* and *Mbp* for oligodendrocytes, as demonstrated by quantitative RT-PCR (qRT-PCR) (Fig. 1*F*).

Cell Type-Specific Translational mRNA Changes Induced by SOD1^{G37R}. Cell type-specific mRNAs recovered from spinal cords of mice with or without the *LoxSOD1*^{G37R} transgene were converted to cDNA libraries and then sequenced. Each biological group contained between three and six sex-matched animals. For each sample, an average of ∼40 million 50-bp reads were uniquely mapped to the annotated mouse (mm9) genome (*SI Appendix*, Table S1). Expression levels for each annotated protein-coding gene were determined by the number of fragments per kilobase of transcript per million mapped reads (FPKM). Genome-wide comparison using unbiased (Spearman) hierarchical clustering of expression levels of mRNAs purified from the three cell types of nontransgenic mice revealed a high correlation between biological replicates of each condition and a clear distinction of mRNAs from motor neurons, astrocytes, oligodendrocytes, and whole spinal cord (*SI Appendix*, Fig. S1). Inspection of scatterplots

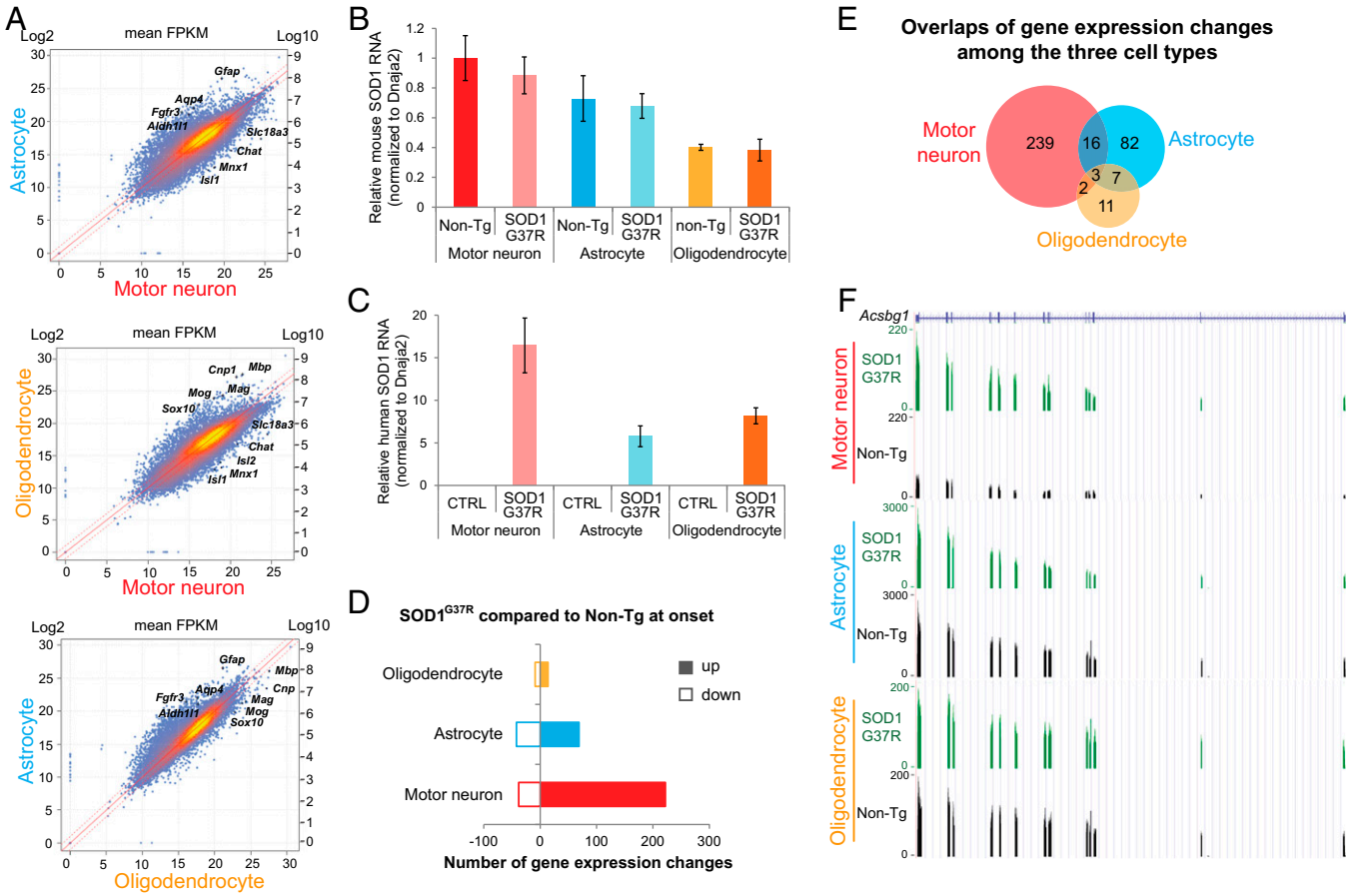

Fig. 2. Cell type-specific transcriptome changes induced by SOD1^{G37R} mutation. (*A*) Scatterplots of average gene expression from multiple biological replicates of immunoprecipitated mRNA from motor neurons versus astrocytes (*Top*), oligodendrocytes versus motor neurons (*Middle*), and astrocytes versus oligodendrocytes (*Bottom*). The dots representing the cell type marker genes are labeled in the figures. (*B*) qRT-PCR of mouse SOD1 in motor neurons, astrocytes, and oligodendrocytes. The relative level is normalized to internal control Dnaja2. Error bars represent SD in three or four biological replicates. (*C*) qRT-PCR of human SOD1 in motor neurons, astrocytes, and oligodendrocytes. The relative level is normalized to internal control Dnaja2. Error bars represent SD in three or four biological replicates. (*D*) Number of gene expression changes in the three cell types, comparing SOD1^{G37R} transgenic mice and nontransgenic mice. (*E*) Number of overlapped gene changes induced by SOD1^{G37R} in motor neurons, astrocytes, and oligodendrocytes. (*F*) RNA-seq reads from SOD1^{G37R} transgenic mice and nontransgenic controls in the three cell types, showing the specific up-regulation of *Acsbg1* mRNA in motor neurons.

of average gene expression from multiple biological replicates of immunoprecipitated mRNA from motor neurons versus astrocytes showed distinct gene expression patterns (Fig. 2*A*, *Top*). A robust enrichment for motor neuron marker genes (*Chat*, *Slc18a3*, *Isl1*, *Isl2*, and *Mnx1*), astrocyte markers (*Aldh1l1*, *Gfap*, *Fgfr3*, and *Aqp4*), or oligodendrocyte markers (*Cnp1*, *Mbp*, *Mog*, *Mag*, and *Sox10*) was found, respectively, in the immunoprecipitated mRNAs from the three cell types (Fig. 2*A*).

Endogenous and mutant SOD1 were expressed at high levels in all three cell types. The endogenous mouse SOD1 mRNA content was highest in motor neurons, with 70% of the motor neuron level found in astrocytes and 40% in oligodendrocytes (Fig. 2*B*). Human SOD1^{G37R} RNA matched the corresponding ratios for mouse SOD1 in motor neurons and oligodendrocytes (100% and 40%, respectively), with mutant SOD1 expressed at only approximately one-half the corresponding endogenous level in astrocytes (30% of the level in motor neurons) (Fig. 2*C*).

We next tested whether gene expression changes were induced in each cell type from expression of mutant SOD1^{G37R}. A genome-wide comparison was performed on RNAs isolated just before disease onset from motor neurons, astrocytes, oligodendrocytes, and whole spinal cord (Fig. 1*B*). An initial unbiased (Spearman) hierarchical clustering of all gene expression values from motor neuron samples was used to determine that all four nontransgenic controls clustered closely together, as expected (*SI Appendix*, Fig. S2*A*). Two of the four SOD1^{G37R} motor neuron samples were well separated from the controls, whereas two others developed more moderated differences with those controls (*SI Appendix*, Fig. S2*A*). Given the variability in age of disease onset across a 100-d window between the mice with the earliest and latest disease onset in this SOD1^{G37R} line (34), we interpret the variability in affected gene expression in the mutant mice to reflect animals with earlier and later disease initiation. Indeed, a heat map of genes with altered expression clearly shows that the two more widely separated mutant animals exhibited more dramatic changes, with more modest changes in the same genes and in the same directions in the remaining two mutant mice (*SI Appendix*, Fig. S2*B*).

We next performed statistical comparisons to identify mRNAs that were changed significantly, using all annotated protein-coding genes (with Cuffdiff FPKM value at least 0.1 in one condition; $q < 0.05$). Near disease onset, the gene expression changes were most dramatic in motor neurons (Fig. 2*D*), with 260 significant changes, ranging from a 50-fold increase in a serotonin transporter (*Slc6a4*) mRNA to a 35% decrease in *Runx2* mRNA *SI Appendix*, Table S2). Fewer changes were seen in astrocyte mRNAs (108 mRNAs altered) and almost no changes were detected in translating oligodendrocyte mRNAs (23 mRNAs altered; a maximum sixfold change). Of note, most of these changes (85% in motor neurons, 62% in astrocytes, and 61% in oligodendrocytes) were up-regulations in expression (with a mean up-regulation of 2.5-fold). Most gene changes were cell type-specific; for example, 239 genes changed only in motor neurons, despite the expression of almost all of them in all three cell types (Fig. 2*E* and *SI Appendix*, Table S9), indicating a unique response by each cell type to mutant SOD1 (synthesized within either it or its cell partners). Furthermore, very few of these changes were identified from an analysis of whole spinal cord RNAs (*SI Appendix*, Fig. S2*C*), reinforcing the value of the bacTRAP method in identifying translational mRNA changes within individual cell types.

Activation of ER Stress in Motor Neurons Expressing Mutant SOD1. Examination of the 260 mRNA changes found in *LoxSOD1^{G37R}* motor neurons revealed a strong enrichment for genes involved in synapses and cell junctions (*SI Appendix*, Table S3). Approximately 10% of all of the gene changes are in this category, consistent with synapse dysfunction accompanying the known denervation that occurs as one of the earliest detected changes in this mouse line (34). Up-regulated gene changes were enriched in genes involved in metabolism, with notable perturbation in the alanine, aspartate, and glutamate metabolism pathways (marked with red stars and red shade in *SI Appendix*, Fig. S3). Down-regulated genes were highly enriched in those encoding ribosomes and components of the translation machinery (*SI Appendix*, Table S3), consistent with disruption of normal overall protein synthesis on ER stress activation.

Analysis of potential transcription factor-binding motifs and coregulatory elements from the total 260 changes in motor neurons revealed two heat-shock proteins, HSF2 and HSF1, and an ER stress responsive transcription factor, CHOP (Fig. 3*A*), strongly indicating UPR activation. The UPR is a major intracellular pathway activated in response to an accumulation of unfolded or misfolded proteins (35, 36). The three branches of the UPR are dependent on cAMP-dependent transcription factor ATF-6 alpha (ATF6), PERK, and IRE1α (a serine/threonine-protein kinase/endoribonuclease). The three branches of the UPR function to sense protein misfolding in the ER and transduce the initial misfolding signal for induction of components of each of the three branches (35, 36). Activation of PERK phosphorylates eIF2α, which enhances the translation of cAMP-dependent transcription factor 4 (ATF4) mRNA (37). Analysis of the mRNAs accumulated within motor neurons at disease onset revealed ER stress, including induction of the ER chaperone PDI and the autophagy component SQSTM1 (p62), and activation of the PERK arm of the UPR pathway, including elevation of ATF4, whose activity in turn induces CHOP (also known as DNA damage-inducible transcript 3 protein), a proapoptotic transcription factor (35). qRT-PCR analysis confirmed elevated levels of CHOP and ATF4 in SOD1^{G37R} motor neurons (Fig. 3*B*). PERK activation was further supported by the ∼2.2-fold enhanced phosphorylation of eIF2α in SOD1^{G37R} motor neurons within lumbar sections of mouse spinal cord at disease onset (Fig. 3 *F* and *G*).

Despite activation of the PERK pathway, neither the ATF6 nor IRE1α pathway of the UPR was similarly activated in motor neurons, as demosnrtated by the absence of changes identified in Bip (also known as Grp78), an ATF6-activated ER chaperone protein, or in X-box-binding protein 1 (XBP1), a key downstream component of the IRE1α pathway (Fig. 3*B*). Furthermore, activation of the IRE1α pathway triggers the RNase activity of IRE1α, which excises a 26-nt intron of the unspliced XBP1 mRNA (XBP1u) to generate an active transcription factor, termed spliced XBP1 (XBP1s) (35). At disease onset, no XBP1s isoform was generated in the motor neurons of the SOD1^{G37R} mice (Fig. 3*B*).

ER stress and activation of the PERK branch of the UPR was found in motor neurons, but not in astrocytes or oligodendrocytes (Fig. 3 *C* and *D*). Analysis of the FPKM values of RNAs encoding ER chaperone proteins in normal motor neurons, astrocytes, and oligodendrocytes revealed much higher expression levels in the two glial cell types than in motor neurons in ER chaperones PDI and FKBP9 (Fig. 3*E*). For example, PDI mRNA levels were approximately 17-fold higher in astrocytes and 12-fold higher in oligodendrocytes compared with motor neurons. Even after a threefold induction in the SOD1^{G37R} motor neurons relative to nontransgenic neurons (Fig. 3*B*), PDI levels remained sixfold below the age-matched levels in normal astrocytes and oligodendroctyes (Fig. 3*E*), consistent with motor neurons being intrinsically more vulnerable to unfolded protein accumulation. FKBP9 levels are similarly elevated by 12-fold in astrocytes and sixfold in oligodendrocytes relative to normal motor neurons (Fig. 3*E*).

To determine whether the selective activation of the PERK arm of the UPR was common to disease-linked SOD1 mutants of different biochemical characters, we examined ER stress components in mice (38) that develop fatal disease from an intrinsically misfolded, dismutase-inactive mutation SOD1^{G85R}

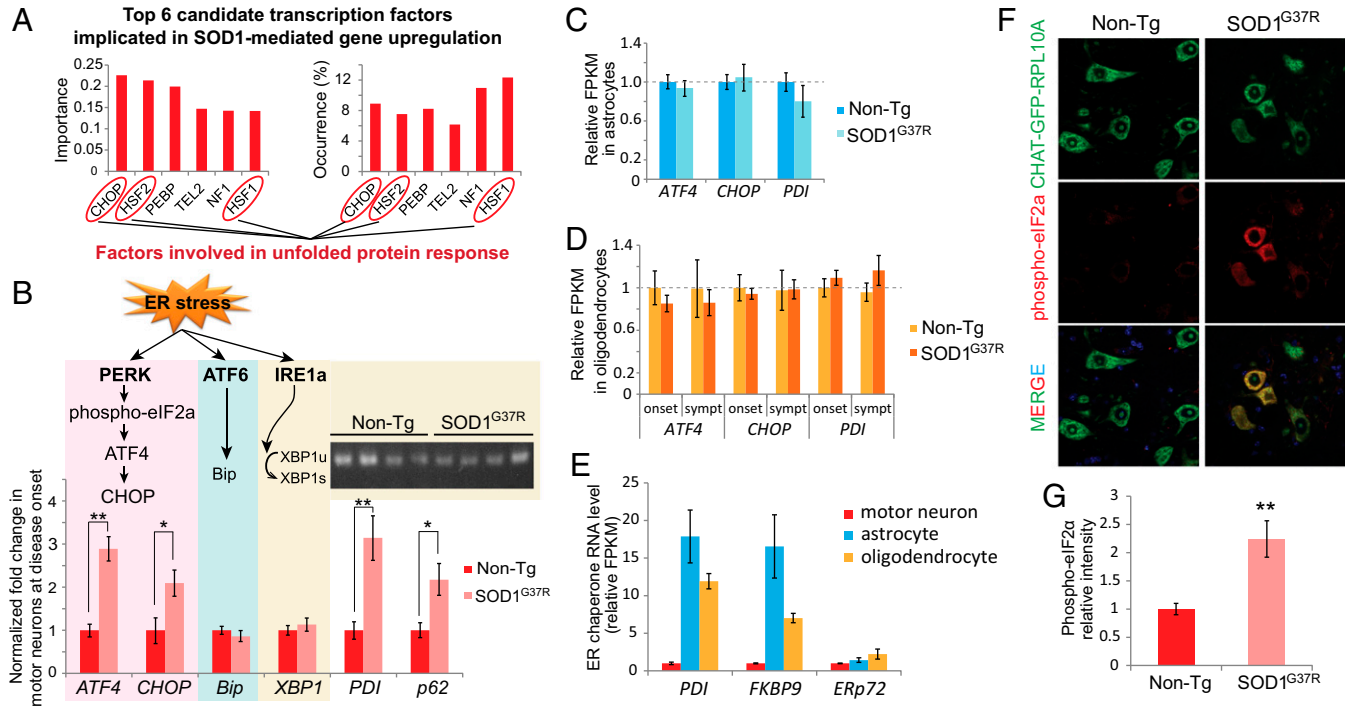

Fig. 3. Activation of ER stress specifically in motor neurons at disease onset. (*A*) Candidate transcription factors of coregulated genes in SOD1 G37R motor neurons, as predicted by the web server DiRE. (*B*) qRT-PCR of genes involved in the UPR-activated ER stress pathway in SOD1 G37R-expressed motor neurons compared with nontransgenic controls. Error bars represent SEM in three or four biological replicates. $*P < 0.05$, $**P < 0.005$, Student *t* test. (*Top*) Schematic diagram of the three branches activated by UPR-induced ER stress. (*Top Right*) RT-PCR of unspliced and spliced isoforms of XBP1 in motor neurons with or without the G37R transgene. (*C*) Relative expression levels of ATF4, CHOP, and PDI in astrocytes at disease onset. The FPKM values from RNA-seq were normalized to those in nontransgenic samples of each gene. Error bars represent SD in four to six biological replicates. (*D*) Relative expression levels (FPKM from RNA-seq) of ATF4, CHOP, and PDI in oligodendrocytes at both onset and an early symptomatic stage. Error bars represent SD in four to six biological replicates. (*E*) Relative expression levels (FPKM) of ER chaperones in the three cell types of nontransgenic mice. The expression levels of each gene were normalized to the value in motor neurons. (*F*) Immunofluorescence of phospho-eIF2α in spinal cords of Chat-EGFP–labeled motor neuron reporter mice, with or without the SOD1^{G37R} transgene. (*G*) Quantification of the intensity of red fluorescence normalized to green fluorescence as in *F*. There were three mice in each group, and approximately 100 motor neurons were quantified in each mouse. Error bars represent SD. $**P < 0.005$, Student *t* test.

(39), which develop slowly progressing disease with modest mutant SOD1 accumulation, similar to the SOD1^{G37R} mouse line except that the mutation is dismutase-inactive. Laser capture microdissection was used to isolate RNAs from motor neurons at an early symptomatic stage (age 10.5 mo). qRT-PCR analysis revealed dramatic elevations of ATF4 expression (40-fold) and CHOP expression (12-fold) (*SI Appendix*, Fig. S2*D*), indicative of activation of the PERK branch of ER stress as a common response in motor neurons induced by dismutase-active and -inactive SOD1 mutations.

Dysfunction of Nuclear Receptors Peroxisome Proliferator-Activated Receptor and Liver X Receptor in Astrocytes Expressing Mutant SOD1. We initially analyzed SOD1-mutant dependent changes in ribosome-bound RNAs recovered from astroctyes using unsupervised Spearman hierarchical clustering of all gene expression values. This analysis revealed that the six nontransgenic controls clustered tightly together, as did three of the four SOD1^{G37R} samples (*SI Appendix*, Fig. S4*A*). As seen in the motor neurons, the majority of the significant RNA changes in astrocytes (67 of 108) were increases, ranging from a 1.8-fold increase for *crem* (cAMP-responsive element modulator) to a 30-fold increase for *Ccl6* (C-C motif chemokine 6) (Fig. 4*A*). There were more modest reductions in 42 RNAs, with the maximum reduction to 33% of the initial level for *Kif20a* (*SI Appendix*, Table S4). Gene ontology analysis revealed enrichment of genes linked to immune responses and with extracellular functions (*SI Appendix*, Table S5), including the chemokine CXCL10 (C-X-C motif chemokine 10) and an insulin-like growth factor-binding protein (IGFBP7), both of which have been shown to have toxic or proapoptotic effects on neurons and in other tissues (40–42). qRT-PCR analysis of RNAs purified from the *Aldh1l1*-promoted EGFP-Rpl10a ribosomes validated fourfold and twofold increases, respectively, in the RNAs encoding CXCL10 and IGFBP7 in the astrocytes from the dismutase-active (SOD1^{G37R}) mutant SOD1 mice (*SI Appendix*, Fig. S4*B*). Similar analyses of RNAs isolated at onset stage from astrocytes of mice that will develop fatal motor paralysis from expressing dismutase-inactive (SOD1^{G85R}) mutant mice showed similar (twofold) increases in CXCL10 and IGFBP7 (*SI Appendix*, Fig. S4*B*).

Although the mRNA levels of the two candidates were unchanged, two families of nuclear receptors, peroxisome proliferator-activated receptor (PPAR) and liver X receptor (LXR), were predicted to be the major transcription coactivators involved in the 108 gene changes in SOD1 mutant-expressing astrocytes (Fig. 4*B*). Both of these proteins can be activated by fatty acid and cholesterol derivatives, and they control the expression of genes involved in metabolism and inflammation (43). On ligand binding, both receptors undergo a conformational change, followed by changes in interacting proteins, and they affect transcription through multiple modes, including direct activation, repression, and transrepression (43, 44). In general, PPAR and LXR activate metabolism and play important roles in energy and lipid homeostasis, and also repress inflammatory gene expression (43, 45) (Fig. 4*C*). In SOD1^{G37R} astrocytes, there was extensive up-regulation of inflammatory gene expression (Fig. 4*D*) and a trend toward a reduction in metabolic genes

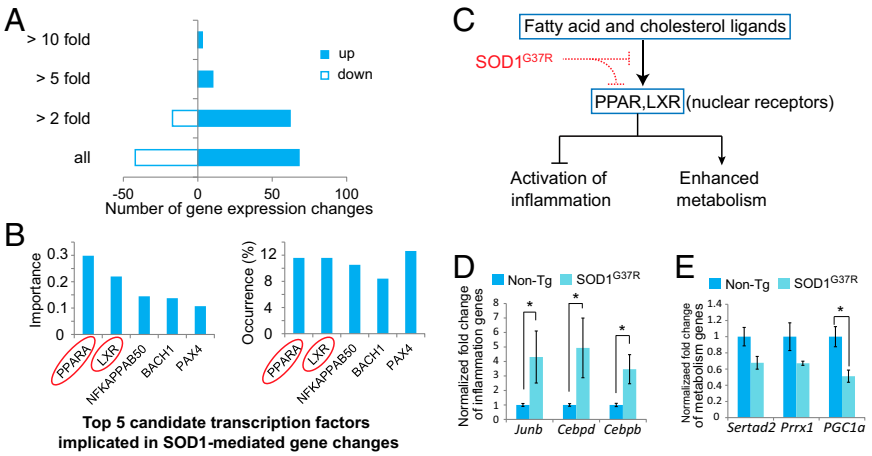

Fig. 4. Gene expression changes in astrocytes at disease onset. (*A*) Number of gene expression changes above 2-, 5-, and 10-fold in SOD1^{G37R} astrocytes at disease onset. (*B*) Candidate transcription factors of coregulated genes in SOD1^{G37R} astrocytes, as predicted by the web server DiRE. (*C*) Diagram of PPAR and LXR functions and how they are altered by the SOD1^{G37R} mutant in astrocytes (red). (*D*) qRT-PCR of inflammatory genes up-regulated in SOD1^{G37R} astrocytes. Error bars represent SEM in three or four biological replicates. *$P < 0.05$, Student *t* test. (*E*) qRT-PCR of genes involved in metabolism down-regulated in G37R astrocytes. Error bars represent SEM in three or four biological replicates. *$P < 0.05$, Student *t* test.

(Fig. 4*E*), several of which have been shown to be targets of PPAR/LXR (46–48).

Along with the apparently increased PPAR/LXR activity, peroxisome proliferator-activated receptor gamma coactivator 1-alpha (PGC1α) was first down-regulated in mutant SOD1^{G37R} astrocytes, but not in motor neurons or oligodendrocytes (Fig. 4*E* and *SI Appendix*, Fig. S4*C*). PGC1α is a transcriptional coactivator of nuclear receptors and other transcription factors that play key roles in mitochondria biogenesis and oxidative metabolism (49, 50). Its expression can be regulated by PPAR, and it also cooperates with PPAR in transcriptional control of nuclear genes encoding mitochondrial fatty acid metabolism (51). A decrease in PGC1α level is not a typical gene expression change accompanying astrogliosis induced by neuroinflammation or stroke (52), suggesting that it may be an intrinsic toxic effect of mutant SOD1 in astrocytes rather than an inflammatory response to the motor neuron dysfunction. Thus, dysfunction of mitochondria and/or oxidative metabolism might account in part for the noncell autonomous toxicity of astrocytes to motor neurons.

Gene Expression Changes in Oligodendrocytes at an Early Symptomatic Stage. The Cnp1-Rpl10a bacTrap approach identified very few changes (only 14 up-regulated and 9 down-regulated RNAs) in SOD1^{G37R} mutant oligodendrocytes at disease onset. Moreover, these changes were smaller in magnitude relative to the changes in motor neurons, ranging from a maximal 2.4-fold increase for *Pla2g4e* (cytosolic phospholipase A2 epsilon) to repression to 37% of the initial level for *Ccne2* (G1/S-specific cyclin-E2) (*SI Appendix*, Table S6).

To test whether changes appeared in oligodendrocytes later in the disease course, we used the Cnp1-Rpl10a bacTrap approach to purify translating RNAs from oligodendrocytes at an early symptomatic disease stage (age 10.5 mo) (Fig. 1*B*). As before, unsupervised hierarchical clustering of all gene expression values revealed that the five nontransgenic controls clustered together, whereas the three SOD1^{G37R} samples were largely distinct from the controls (*SI Appendix*, Fig. S5*A*). A total of 750 gene expression changes were identified in annotated protein-coding genes (with a cuffdiff FPKM value of at least 0.1 in one condition; $q < 0.05$; Fig. 5*A*), 628 of which were up-regulated (between 1.7- and 33-fold) (*SI Appendix*, Table S7). A total of 439 genes were up-regulated at least twofold, 92 genes were up-regulated more than fivefold, and 12 genes were up-regulated more than 10-fold (Fig. 5*B*). The use of qRT-PCR to provide an independent assessment of RNA levels validated the changes in RNA levels (Fig. 5*C*). Fourteen of the 23 RNA changes seen at disease onset showed enhanced dysregulation at an early symptomatic stage (*SI Appendix*, Table S7).

Gene ontology analysis revealed that membrane protein-encoding genes were disproportionately misregulated, composing ∼25% of the up-regulated RNAs and 45% of the down-regulated RNAs (*SI Appendix*, Table S8). Furthermore, all three main proteins composing the myelin sheath—myelin basic protein (MBP), myelin oligodendrocyte glycoprotein (MOG), and proteolipid protein (Plp1)—were down-regulated in the SOD1^{G37R} oligodendrocytes (Fig. 5*D*). In addition, RNAs encoding components of three major signaling pathways—phosphatidylinositol signaling ($P = 0.0008$, Benjamini test), FcγR-mediated phagocytosis ($P = 0.0007$, Benjamini test) and a calcium signaling pathway ($P = 0.0009$, Benjamini test)— were perturbed (*SI Appendix*, Figs. 6 and 7). Members of phosphoinositide phospholipase C (PLC) and Ca^{2+}/calmodulin-dependent protein kinase (CaMK) protein families were up-regulated. PLCs participate in phosphatidylinositol 4,5-bisphosphate (PIP_2) metabolism and lipid signaling pathways in a calcium-dependent manner, and are essential for intracellular calcium homeostasis (53). CaMK is a serine/threonine-specific protein kinase regulated by the Ca^{2+}/calmodulin complex that has been shown to regulate oligodendrocyte maturation and myelination (54). Strikingly, nine of the 15 members of the PLC family and six CaMKs were up-regulated in oligodendrocytes in SOD1^{G37R} mice at this early symptomatic stage (Fig. 5 *E* and *F*). Similar analysis of RNAs from oligodendrocytes of SOD1^{G85R} mice isolated using the Cnp1-Rpl10a bacTrap approach at early symptomatic stage revealed a similar trend of changes (albeit of lower magnitude) in the two gene families (*SI Appendix*, Fig. 5 *B* and *C*), indicating common defects from dismutase-active and -inactive SOD1 mutants.

It was previously reported that the main lactate transporter, monocarboxylate transporter 1 (MCT1), which provides metabolic support to axons, was suppressed in oligodendrocytes of SOD1^{G93A} mice (55). Surprisingly, however, despite 750 altered RNAs, changes in MCT1 mRNAs were not seen in oligodendrocytes at either disease onset or the early symptomatic stage in either SOD1^{G37R} or SOD1^{G85R} mutant mice (*SI Appendix*, Fig. S5*D*). Thus, altered levels of MCT1 synthesis (e.g., translating mRNAs) cannot be an early damaging factor that drives initiation of non–cell-autonomous toxicity from oligodendrocytes to motor neurons.

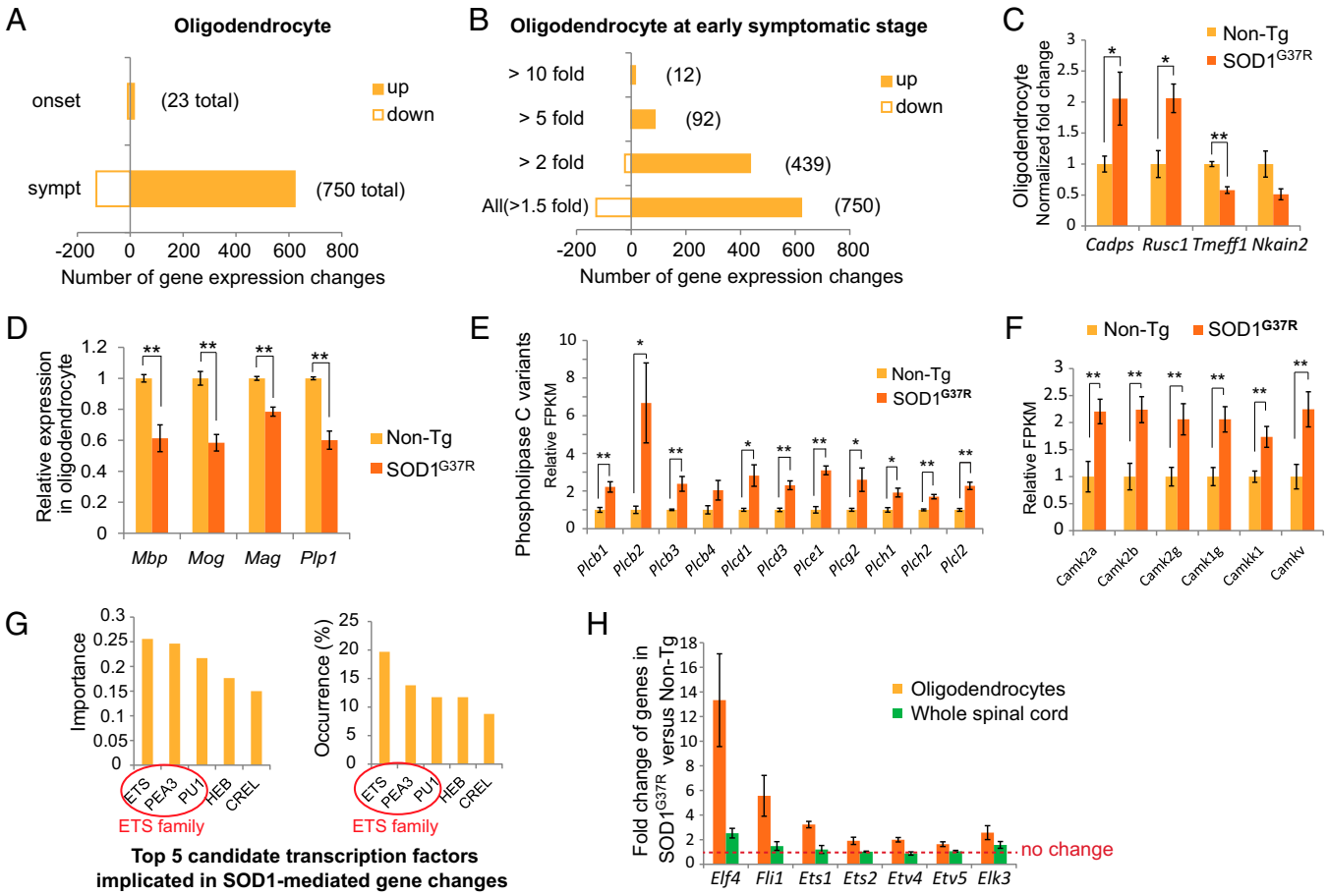

Fig. 5. Gene expression changes in oligodendrocytes. (*A*) Number of gene expression changes in oligodendrocytes at disease onset and early symptomatic stage, comparing SOD1^{G37R} transgenic mice with nontransgenic mice. (*B*) Number of gene expression changes above 2-, 5-, and 10-fold in SOD1^{G37R} oligodendrocytes at an early symptomatic stage. (*C*) qRT-PCR validation of gene changes in SOD1^{G37R} oligodendrocytes at early symptomatic stage. Error bars represent SEM in three or four biological replicates. $*P < 0.05$, $**P < 0.005$, Student *t* test. (*D–F*) Relative expression levels of myelin proteins (*D*), PLC family genes (*E*), and CaMK genes (*F*) in oligodendrocytes at early symptomatic stage. The FPKM values were normalized to values in nontransgene samples for each gene. Error bars represent SD in three to five biological replicates. $*P < 0.05$, $**P < 0.005$, Student *t* test. (*G*) Candidate transcription factors of coregulated genes in SOD1^{G37R} olidodendrocytes, as predicted by the web server DiRE. (*H*) Fold change of ETS transcription factors in SOD1^{G37R} oligodendrocytes or whole spinal cord compared with those in nontransgenic controls. The FPKM values were normalized to values in nontransgene samples for each gene. Error bars represent SD in three to five biological replicates.

Our analysis of potential binding motifs and coregulatory elements identified four subfamilies of the ETS transcription factors—ETS, PEA3, PU1 (SPI), and ELF—as candidate transcription factors whose elevated activity could underlie increased expression of 427 of the 622 genes with greater than twofold changes in mutant-expressing oligodendrocytes (Fig. 5*G*). The ETS (E26 transformation-specific or E-twenty-six) family is one of the largest families of transcription factors in mice, with 12 subfamilies and 28 total members (56, 57). RNAs encoding seven of these factors were significantly up-regulated in SOD1^{G37R} oligodendrocytes, with two (Elf4 and Fli1) increased by more than fivefold (Fig. 5*H*). Elevated levels of these RNAs (elevated to a smaller extent) were also identified at early symptomatic stage in SOD1^{G85R} oligodendrocytes (*SI Appendix*, Fig. S5*E*).

Functional gene ontology analysis with candidate ETS targets in the SOD1 mutant-mediated expression-changed genes revealed significant elevations in genes in the phosphatidylinositol signaling system ($P = 0.005$, Benjamini test) and FcγR-mediated phagocytosis ($P = 0.000008$, Benjamini test) (*SI Appendix*, Fig. S6 *A* and *B*). Phagocytosis is a major mechanism for removing pathogens and cell debris. It was once thought to be carried out mainly by microglia in the CNS (58), but recently was found to be performed by astrocytes as well, for synapse and neuronal debris elimination (59, 60).

As a further test to confirm that the changes identified in translating RNAs from oligodendrocytes are not likely to be remaining RNA contaminants from large changes in microglia or astroctyes, we examined the fold changes of genes in the FcγR-mediated phagocytosis pathway in whole spinal cord. Up-regulation was either not observed or observed at a much smaller magnitude compared with that in oligodendrocyte-derived RNAs (*SI Appendix*, Fig. S5*F*), consistent with increased synthesis in phagocytosis components within oligodendrocytes. Although we are unaware of any reported evidence of phagocytosis in oligodendrocytes, Fc receptor mediated-signaling has been implicated in the induction of oligodendrocyte differentiation and myelination (61).

Discussion

Motor neuron degeneration caused by mutant SOD1 is non–cell-autonomous (14), with contributions from neighboring glia cells (3–5, 7–9, 11), but no consensus has been reached on the precise mechanisms involved. To examine this question, we combined ribosome tagging in mice (bacTRAP) to enable isolation of cell type-specific polyribosome-associated mRNAs in the context of intact neuronal-glial networks with high-throughput sequencing (RNA-seq). Starting with RNAs isolated from mice ubiquitously expressing

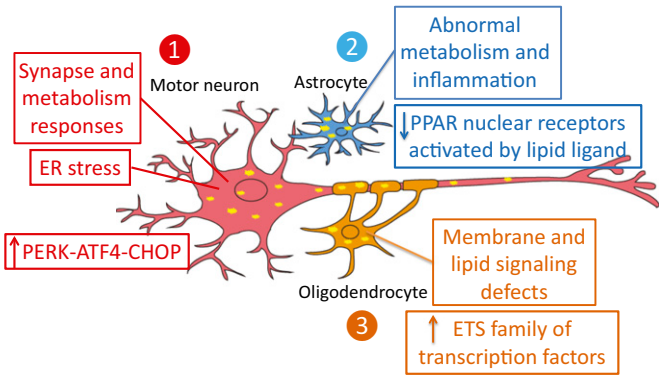

Fig. 6. Cell type-specific toxicity of mutant SOD1 in motor neurons, astrocytes, and oligodendrocytes. (1) Initial damage occurs in motor neurons at disease onset, including synapse and metabolism responses and activation of ER stress. (2) Damage in astrocytes includes abnormal metabolism and inflammation, owing in part to the dysfunction of PPAR and LXR nuclear receptors that are activated by lipid ligands. (3) Damage in oligodendrocytes occurs in an early symptomatic stage, later than that in motor neurons and astrocytes. The toxicity includes mainly myelination and lipid signaling defects, coupled with activation of the ETS family of transcription factors.

dismutase-active or -inactive mutant SOD1 at or just before disease onset, we identified early events within motor neurons, followed by later RNA dysregulation in astrocytes and oligodendrocytes.

Early RNA expression changes identified in mutant SOD1-expressing motor neurons include ER stress, synapse, and metabolic abnormalities (Fig. 6). Few RNA changes were initially found in astrocytes, with many accumulating later, including in genes involved in inflammation and metabolism, enriched for targets of PPAR and LXR nuclear receptors (Fig. 6). This finding is consistent with earlier efforts using genetic deletion of mutant SOD1 from motor neurons to delay disease onset (5, 7), whereas similar deletion from astrocytes slowed disease progression with no strong effect on onset (8, 9). Curiously, although mutant SOD1 gene inactivation in $NG2^{+}$ progenitor oligodendrocytes reportedly delays the age of disease onset (11), with only a modest effect in slowing progression after onset in $SOD1^{G37R}$ mice, our genomic data show hardly any changes in oligodendrocytes at this age, with dramatic changes arising by an early symptomatic stage, consisting mainly of dysregulation of myelination and lipid signaling pathways coupled with activation of ETS transcription factors (Fig. 6). The strong effect on disease onset from removal of mutant SOD1 from $NG2^{+}$ cells implies that they may have additional functional roles or are progenitors of additional cell populations beyond a role as the in vivo progenitors of mature Cnp1-expressing oligodendrocytes.

Activation of ER stress has been implicated in the pathogenesis of ALS (62–66). Up-regulation of Bip (downstream of the ATF6 branch) was initially reported in cell cultures transfected with mutant SOD1 and spinal cords of transgenic $SOD1^{H46R}$ and $SOD1^{L84V}$ mice (64). Another study at disease onset in $SOD1^{G93A}$ mice reported increased activity of CHOP, a downstream target indicating activation of the PERK branch of the UPR (66). Activation of all three arms of the UPR with activated ATF6, ATF4, and XBP1 found in spinal cords, but not cerebellum, has been reported in end-stage $SOD1^{G93A}$ and $SOD1^{G85R}$ mice (63). Adding to this knowledge, we have established that ER stress starts within motor neurons with selective activation of the PERK-ATF4-eIF2α pathway, leading to up-regulation of CHOP and its transcriptional targets, and have further confirmed the specific activation of its upstream regulators at disease onset. This finding adds an in vivo example during disease pathogenesis to previous cell culture evidence establishing that the three UPR sensors can have fundamental differences in the timing of their signaling and responses to particular ER stress stimuli (35, 67). Our data establish that chronic accumulation of misfolded SOD1 initiates activation of the PERK branch of ER stress selectively in postmitotic motor neurons, but not in astrocytes or oligodendrocytes even at symptomatic disease stages, supporting a special vulnerability of motor neurons to misfolded SOD1 accumulation. One simple explanation for this vulnerability is our identification of highly divergent levels of ER chaperones, with much higher levels in astrocytes and oligodendrocytes than in motor neurons.

Furthermore, immunostaining of phospho-eIF2α within individual motor neurons has revealed that some motor neurons develop ER stress activation earlier than others, consistent with report of ER stress activation in selectively vulnerable motor neuron subtypes (68). A recent cell culture study also reported ER stress in both IREα and PERK branches induced by mutant SOD1 in immature induced pluripotent cells (iPSC)-derived motor neurons, with the basal level of ER stress (reported by spliced Xbp1) inherently higher in healthy motor neurons compared with other neurons and nonneuronal cell types in in vitro cultures (69). The differences between our in vivo findings of selective PERK pathway activation compared with broader ER stress activation in cell cultures (spliced Xbp1) (Fig. 3*B*) likely reflect the additive effects of those from mutant SOD1 and the stressed environment facing cells in cell cultures. ER stress is usually triggered by the accumulation of misfolded proteins within the ER lumen. Although SOD1 is not a secreted protein and is not synthesized inside the ER lumen, mutant SOD1 has been shown to directly interact with Derlin-1, a component of the ER-associated degradation (ERAD) machinery, and activates ER stress through dysfunction of ERAD (70). It also has been shown that misfolded SOD1 has increased association with mitochondria and ER membranes (71–75). Furthermore, the conformation of membrane-associated mutant SOD1 has been solved by NMR, revealing that the association is mediated by interfacial amphiphilic helices (76). Based on the foregoing findings, we propose that the abnormal insertion of misfolded SOD1 onto/into ER membranes in motor neurons interferes with the normal function of other membrane proteins, including protein folding, modification, and degradation, with activation of the PERK pathway of ER stress from direct SOD1 mutant damage to Derlin or indirect damage from disrupted protein homeostasis.

Whether manipulation of the ER stress pathways can provide a protective effect remains controversial. Breeding with $ATF4^{-/-}$ mice (77) or nervous system deletion of XBP-1 (78) has been reported to modestly delay disease onset and/or prolong the life span, but only in one-half of $SOD1^{G86R}$ mice studied; however, crossing with $PERK^{+/-}$ mice has been reported to accelerate disease onset and shorten life span in $SOD1^{G85R}$ mice (79). The ER stress-protective agent salubrinal, an inhibitor of eIF2α dephosphorylation, has been shown to mitigate disease progression (68). Furthermore, eIF2α phosphorylation was found to be up-regulated by TDP-43 toxicity in flies, and a PERK inhibitor could attenuate its damage in flies and mammalian neurons (80). Therefore, disturbance of ER proteostasis might be a more general phenomenon underlying the selective motor neuron degeneration caused by different mutant genes in ALS. The divergent findings produce a complex scenario regarding therapy development, with intervention at different steps of the ER stress pathways, at different timings and under different circumstances, or on different cell types apparently resulting in opposite effects on the neurodegeneration process.

Finally, our bac-Trap approach has identified a temporal cascade of different cellular pathways activated by mutant SOD1 in motor neurons, astrocytes, and oligodendrocytes. ER stress activated in motor neurons is an initiating event, presumably mediated by activation of a UPR sensor on ER membranes. Altered lipid signaling is seen in all three cell types. PPAR and LXR nuclear receptors that are normally activated by fatty acid and cholesterol derivatives were predicted to be dysfunctional in

astrocytes. Extensive membrane proteins and lipid signaling pathways were subsequently dysregulated in oligodendrocytes. Taken together, the collective evidence supports the idea that the toxicity of misfolded SOD1 originates from its abnormal membrane association. With aging, a decreasing ability to degrade unfolded proteins leads to increasing associations of mutant SOD1 with different membranes and eventually initiates a cascade of cellular responses and gene expression changes that result in motor neuron dysfunction and death. Owing to the distinctive intrinsic properties of the different cell types, this common toxic feature provokes cell type-specific responses that contribute to disease initiation and progression in a coordinated manner. Motor neurons are most vulnerable to the accumulated mutant SOD1 and abnormal cellular pathways because they synthesize high levels of SOD1 and have very low levels of ER chaperones. Subsequent damage developed from mutant SOD1 synthesis within astrocytes and oligodendrocytes is essential for amplifying the initial damage within motor neurons.

Materials and Methods

Animals. ALS mouse lines SOD1^{G37R} (5), SOD1^{G85R} (38), and SOD1^{G93A} (19) are all heterozygous for a 12-kb genomic DNA fragment encoding the human mutant SOD1 transgene, under its endogenous promoter. The bacTRAP transgenic mouse line *Chat*-bacTRAP line expresses an EGFP-tagged ribosome protein Rpl10a only within motor neurons. The *Aldh1l1*-bacTRAP line expresses the same EGFP-tagged Rpl10a in astrocytes, whereas the *Cnp1*-bacTRAP expresses it in oligodendrocytes (28, 29). All animal experiments used in this work were approved by the University of California at San Diego Institutional Animal Care and Use Committee.

Purification of Cell Type-Specific mRNA from bacTRAP Mice. Dissected mouse spinal cord was immediately homogenized in ice-cold polysome extraction buffer (20 mM Hepes pH 7.4, 150 mM KCl, 5 mM $MgCl_2$, 0.5 mM DTT, 100 μg/mL cycloheximide, protease inhibitors, and RNase inhibitors). Homogenates were centrifuged at 2,000 × *g* for 10 min at 4 °C, after which Nonidet P-40 and 1,2-diheptanoyl-sn-glycero-3-phosphocholine (Avanti Polar Lipids) were added to the supernatant at final concentrations of 1% and 30 mM. The lysates were centrifuged at 13,000 × *g* for 15 min at 4 °C after incubation on ice for 5 min. Two monoclonal GFP antibody (Htz-GFP19C8 and Htz-GFP19F7; Memorial Sloan Kettering Cancer Center Monoclonal Antibody Core Facility)-coated magnetic beads (Dynabeads Protein G; Invitrogen) were added to the supernatant, followed by incubation at 4 °C with rotation overnight. Beads were subsequently washed five times with high-salt polysome wash buffer (20 mM Hepes pH 7.4, 350 mM KCl, 5 mM $MgCl_2$, 0.5 mM DTT, 1% Nonidet P-40, and 100 μg/mL cycloheximide). The RNA bound on the beads were extracted with an Absolutely RNA Nanoprep Kit (Stratagene) and quantified by the RiboGreen RNA assay (Invitrogen).

RNA-seq Library Preparation and Transcriptome Analysis. RNA quality was measured using the Agilent Bioanalyzer system according to the manufacturer's recommendations. RNA-seq libraries were prepared from RNAs extracted from specific cell types or whole spinal cord, using an Illumina TruSeq RNA Sample Preparation Kit. RNA-seq libraries were sequenced on an Illumina HiSEq 2000 sequencer for 50 cycles from a single end.

The reads were aligned to a reference mouse genome obtained from the University of California Santa Cruz (mm9; NCBI build 37) using Tophat (default parameters, with the exception of reporting reads mapping to unique locations on the reference) (81). RNA-seq results were visualized in the UCSC Genome Browser (genome.ucsc.edu/) by generating custom tracks using bigwig files. The relative abundance of transcripts was measured by FPKM using Cufflinks (82). Expression variations of protein-coding genes between nontrangenic control and mutant SOD1 groups were quantified and compared by cuffdiff (83). Scatterplots, heat maps, and hierarchical clustering were generated by R software using FPKM values from each sample. Gene ontology analysis was performed using DAVID (https://david.ncifcrf.gov/). Distant regulatory elements of coregulated genes were analyzed by DiRE (dire.dcode.org/).

Laser Capture Microdissection. Mice were perfused with sterile ice-cold PBS. Spinal cords were dissected, incubated in 20% (wt/vol) sucrose (in PBS) at 4 °C overnight, and subsequently embedded in optimal cutting temperature (OCT) compound (Sakura) and frozen in isopentane cooled to −40 °C on dry ice. Tissues were cut into 14-μm sections and stained with Cresyl violet. Approximately 700 motor neurons were laser capture microdissected from each mouse, and RNA was extracted using the RNAqueous-Micro Kit (Ambion) and amplified using the MessageAmp II aRNA amplification kit (Ambion).

qRT-PCR. For first-strand cDNA synthesis, random hexamers were used with a high-capacity cDNA reverse transcription kit (Applied Biosystems). qRT-PCR reactions were performed with three or four biological replicates for each group and two technical replicates using iQ SYBR Green Supermix (Bio-Rad) on the iQ5 Multicolor Real-Time PCR system (Bio-Rad). The data were analyzed using iQ5 optical system software, version 2.1 (Bio-Rad). Expression values were normalized to the control genes *Rpl23* and *Dnaja2*. Intergroup differences were assessed using the two-tailed Student *t* test. Primer sequences are presented in *SI Appendix*, Table S10.

Immunofluorescence. Mice were perfused intracardially with 4% (vol/vol) paraformaldehyde in 0.1 M Sorenson's phosphate buffer, pH 7.2. The entire spinal cord was dissected, postfixed for 2 h in fixative, and the transferred in a 30% sucrose phosphate buffer for at least 2 d. The lumbar spinal cord was embedded in OCT compound and snap-frozen in isopentane cooled to −40 °C on dry ice. Floating lumbar spinal cord cryosections (30 μm) were incubated in a blocking solution containing PBS, 0.5% Tween 20, and 1.5% (wt/vol) BSA for 1 h, 30 min at room temperature and then in PBS and 0.3% Triton X-100 overnight at room temperature, with the following primary polyclonal antibodies against ChAT (Millipore), GFAP (Dako), CC1 (Calbiochem), GFP (a gift from the Oegema/Desai laboratory), and phosphor-eIF2α (Cell Signaling Technology). Primary antibodies were washed with PBS and then detected using FITC or Cy3-coupled secondary antibodies (Jackson ImmunoResearch). The sections were washed with PBS and mounted. Analysis was performed using a Nikon Eclipse laser scanning confocal microscope. Fluorescence intensity from unsaturated images captured with identical confocal settings (a minimum of six spinal cord sections imaged per animal) was quantified using NIS-Elements software (Nikon).

ACKNOWLEDGMENTS. We thank Drs. Nathaniel Heintz and Jeffery Rothstein for the bacTRAP reporter mice; Dr. Myriam Heiman for the detailed protocol for the bacTRAP RNA purification method; members of B. Ren's laboratory, especially Z. Ye, S. Kuan, and B. Li, for technical help with the Illumina sequencing; and all members of the D.W.C. laboratory for critical comments and helpful suggestions. This work was supported by National Institutes of Health Grant R01 NS27036 (to D.W.C.). S.S. was a recipient of the Milton Safenowitz Postdoctoral Fellowship from the ALS Association, a Target ALS Springboard Fellowship, and a National Institutes of Health K99/R00 Award (NS091538-01).

1. Boillée S, Vande Velde C, Cleveland DW (2006) ALS: A disease of motor neurons and their nonneuronal neighbors. *Neuron* 52(1):39–59.
2. Rosen DR (1993) Mutations in Cu/Zn superoxide dismutase gene are associated with familial amyotrophic lateral sclerosis. *Nature* 362(6415):59–62.
3. Clement AM, et al. (2003) Wild-type nonneuronal cells extend survival of SOD1 mutant motor neurons in ALS mice. *Science* 302(5642):113–117.
4. Yamanaka K, et al. (2008) Mutant SOD1 in cell types other than motor neurons and oligodendrocytes accelerates onset of disease in ALS mice. *Proc Natl Acad Sci USA* 105(21):7594–7599.
5. Boillée S, et al. (2006) Onset and progression in inherited ALS determined by motor neurons and microglia. *Science* 312(5778):1389–1392.
6. Kang SH, Fukaya M, Yang JK, Rothstein JD, Bergles DE (2010) NG2$^+$ CNS glial progenitors remain committed to the oligodendrocyte lineage in postnatal life and following neurodegeneration. *Neuron* 68(4):668–681.
7. Wang L, Sharma K, Grisotti G, Roos RP (2009) The effect of mutant SOD1 dismutase activity on non-cell autonomous degeneration in familial amyotrophic lateral sclerosis. *Neurobiol Dis* 35(2):234–240.
8. Yamanaka K, et al. (2008) Astrocytes as determinants of disease progression in inherited amyotrophic lateral sclerosis. *Nat Neurosci* 11(3):251–253.
9. Wang L, Gutmann DH, Roos RP (2011) Astrocyte loss of mutant SOD1 delays ALS disease onset and progression in G85R transgenic mice. *Hum Mol Genet* 20(2):286–293.
10. Lobsiger CS, Cleveland DW (2007) Glial cells as intrinsic components of non–cell-autonomous neurodegenerative disease. *Nat Neurosci* 10(11):1355–1360.
11. Kang SH, et al. (2013) Degeneration and impaired regeneration of gray matter oligodendrocytes in amyotrophic lateral sclerosis. *Nat Neurosci* 16(5):571–579.
12. Ilieva H, Polymenidou M, Cleveland DW (2009) Non-cell autonomous toxicity in neurodegenerative disorders: ALS and beyond. *J Cell Biol* 187(6):761–772.
13. Perrin FE, et al. (2005) No widespread induction of cell death genes occurs in pure motoneurons in an amyotrophic lateral sclerosis mouse model. *Hum Mol Genet* 14(21):3309–3320.
14. Lobsiger CS, Boillée S, Cleveland DW (2007) Toxicity from different SOD1 mutants dysregulates the complement system and the neuronal regenerative response in ALS motor neurons. *Proc Natl Acad Sci USA* 104(18):7319–7326.

15. Ferraiuolo L, et al. (2007) Microarray analysis of the cellular pathways involved in the adaptation to and progression of motor neuron injury in the SOD1 G93A mouse model of familial ALS. *J Neurosci* 27(34):9201–9219.
16. Ferraiuolo L, et al. (2011) Dysregulation of astrocyte-motoneuron cross-talk in mutant superoxide dismutase 1-related amyotrophic lateral sclerosis. *Brain* 134(Pt 9):2627–2641.
17. Bandyopadhyay U, et al. (2013) RNA-seq profiling of spinal cord motor neurons from a presymptomatic SOD1 ALS mouse. *PLoS One* 8(1):e53575.
18. Chiu IM, et al. (2013) A neurodegeneration-specific gene-expression signature of acutely isolated microglia from an amyotrophic lateral sclerosis mouse model. *Cell Reports* 4(2):385–401.
19. Gurney ME, et al. (1994) Motor neuron degeneration in mice that express a human Cu,Zn superoxide dismutase mutation. *Science* 264(5166):1772–1775.
20. Di Giorgio FP, Carrasco MA, Siao MC, Maniatis T, Eggan K (2007) Non-cell autonomous effect of glia on motor neurons in an embryonic stem cell-based ALS model. *Nat Neurosci* 10(5):608–614.
21. Di Giorgio FP, Boulting GL, Bobrowicz S, Eggan KC (2008) Human embryonic stem cell-derived motor neurons are sensitive to the toxic effect of glial cells carrying an ALS-causing mutation. *Cell Stem Cell* 3(6):637–648.
22. Haidet-Phillips AM, et al. (2011) Astrocytes from familial and sporadic ALS patients are toxic to motor neurons. *Nat Biotechnol* 29(9):824–828.
23. Marchetto MC, et al. (2008) Non–cell-autonomous effect of human SOD1 G37R astrocytes on motor neurons derived from human embryonic stem cells. *Cell Stem Cell* 3(6):649–657.
24. Nagai M, et al. (2007) Astrocytes expressing ALS-linked mutated SOD1 release factors selectively toxic to motor neurons. *Nat Neurosci* 10(5):615–622.
25. Meyer K, et al. (2014) Direct conversion of patient fibroblasts demonstrates non-cell autonomous toxicity of astrocytes to motor neurons in familial and sporadic ALS. *Proc Natl Acad Sci USA* 111(2):829–832.
26. Frakes AE, et al. (2014) Microglia induce motor neuron death via the classical NF-κB pathway in amyotrophic lateral sclerosis. *Neuron* 81(5):1009–1023.
27. Phatnani HP, et al. (2013) Intricate interplay between astrocytes and motor neurons in ALS. *Proc Natl Acad Sci USA* 110(8):E756–E765.
28. Heiman M, et al. (2008) A translational profiling approach for the molecular characterization of CNS cell types. *Cell* 135(4):738–748.
29. Doyle JP, et al. (2008) Application of a translational profiling approach for the comparative analysis of CNS cell types. *Cell* 135(4):749–762.
30. Da Cruz S, et al. (2012) Elevated PGC-1α activity sustains mitochondrial biogenesis and muscle function without extending survival in a mouse model of inherited ALS. *Cell Metab* 15(5):778–786.
31. Zhong Z, et al. (2009) Activated protein C therapy slows ALS-like disease in mice by transcriptionally inhibiting SOD1 in motor neurons and microglia cells. *J Clin Invest* 119(11):3437–3449.
32. Bushong EA, Martone ME, Ellisman MH (2004) Maturation of astrocyte morphology and the establishment of astrocyte domains during postnatal hippocampal development. *Int J Dev Neurosci* 22(2):73–86.
33. Molofsky AV, et al. (2012) Astrocytes and disease: A neurodevelopmental perspective. *Genes Dev* 26(9):891–907.
34. Parone PA, et al. (2013) Enhancing mitochondrial calcium buffering capacity reduces aggregation of misfolded SOD1 and motor neuron cell death without extending survival in mouse models of inherited amyotrophic lateral sclerosis. *J Neurosci* 33(11):4657–4671.
35. Hetz C (2012) The unfolded protein response: Controlling cell fate decisions under ER stress and beyond. *Nat Rev Mol Cell Biol* 13(2):89–102.
36. Walter P, Ron D (2011) The unfolded protein response: From stress pathway to homeostatic regulation. *Science* 334(6059):1081–1086.
37. Harding HP, et al. (2000) Regulated translation initiation controls stress-induced gene expression in mammalian cells. *Mol Cell* 6(5):1099–1108.
38. Bruijn LI, et al. (1997) ALS-linked SOD1 mutant G85R mediates damage to astrocytes and promotes rapidly progressive disease with SOD1-containing inclusions. *Neuron* 18(2):327–338.
39. Borchelt DR, et al. (1994) Superoxide dismutase 1 with mutations linked to familial amyotrophic lateral sclerosis possesses significant activity. *Proc Natl Acad Sci USA* 91(17):8292–8296.
40. van Weering HR, et al. (2011) CXCL10/CXCR3 signaling in glia cells differentially affects NMDA-induced cell death in CA and DG neurons of the mouse hippocampus. *Hippocampus* 21(2):220–232.
41. Sui Y, et al. (2006) CXCL10-induced cell death in neurons: Role of calcium dysregulation. *Eur J Neurosci* 23(4):957–964.
42. Wajapeyee N, Serra RW, Zhu X, Mahalingam M, Green MR (2008) Oncogenic BRAF induces senescence and apoptosis through pathways mediated by the secreted protein IGFBP7. *Cell* 132(3):363–374.
43. Hong C, Tontonoz P (2008) Coordination of inflammation and metabolism by PPAR and LXR nuclear receptors. *Curr Opin Genet Dev* 18(5):461–467.
44. Glass CK, Rosenfeld MG (2000) The coregulator exchange in transcriptional functions of nuclear receptors. *Genes Dev* 14(2):121–141.
45. Li AC, Glass CK (2004) PPAR- and LXR-dependent pathways controlling lipid metabolism and the development of atherosclerosis. *J Lipid Res* 45(12):2161–2173.
46. Lemay DG, Hwang DH (2006) Genome-wide identification of peroxisome proliferator response elements using integrated computational genomics. *J Lipid Res* 47(7):1583–1587.
47. Pehkonen P, et al. (2012) Genome-wide landscape of liver X receptor chromatin binding and gene regulation in human macrophages. *BMC Genomics* 13:50–70.
48. Boergesen M, et al. (2012) Genome-wide profiling of liver X receptor, retinoid X receptor, and peroxisome proliferator-activated receptor α in mouse liver reveals extensive sharing of binding sites. *Mol Cell Biol* 32(4):852–867.
49. Finck BN, Kelly DP (2006) PGC-1 coactivators: inducible regulators of energy metabolism in health and disease. *J Clin Invest* 116(3):615–622.
50. St-Pierre J, et al. (2006) Suppression of reactive oxygen species and neurodegeneration by the PGC-1 transcriptional coactivators. *Cell* 127(2):397–408.
51. Vega RB, Huss JM, Kelly DP (2000) The coactivator PGC-1 cooperates with peroxisome proliferator-activated receptor alpha in transcriptional control of nuclear genes encoding mitochondrial fatty acid oxidation enzymes. *Mol Cell Biol* 20(5):1868–1876.
52. Zamanian JL, et al. (2012) Genomic analysis of reactive astrogliosis. *J Neurosci* 32(18):6391–6410.
53. Meldrum E, Parker PJ, Carozzi A (1991) The PtdIns-PLC superfamily and signal transduction. *Biochim Biophys Acta* 1092(1):49–71.
54. Waggener CT, Dupree JL, Elgersma Y, Fuss B (2013) CaMKIIβ regulates oligodendrocyte maturation and CNS myelination. *J Neurosci* 33(25):10453–10458.
55. Lee Y, et al. (2012) Oligodendroglia metabolically support axons and contribute to neurodegeneration. *Nature* 487(7408):443–448.
56. Gutierrez-Hartmann A, Duval DL, Bradford AP (2007) ETS transcription factors in endocrine systems. *Trends Endocrinol Metab* 18(4):150–158.
57. Hollenhorst PC, McIntosh LP, Graves BJ (2011) Genomic and biochemical insights into the specificity of ETS transcription factors. *Annu Rev Biochem* 80:437–471.
58. Brown GC, Neher JJ (2014) Microglial phagocytosis of live neurons. *Nat Rev Neurosci* 15(4):209–216.
59. Chung WS, et al. (2013) Astrocytes mediate synapse elimination through MEGF10 and MERTK pathways. *Nature* 504(7480):394–400.
60. Tasdemir-Yilmaz OE, Freeman MR (2014) Astrocytes engage unique molecular programs to engulf pruned neuronal debris from distinct subsets of neurons. *Genes Dev* 28(1):20–33.
61. Nakahara J, et al. (2003) Signaling via immunoglobulin Fc receptors induces oligodendrocyte precursor cell differentiation. *Dev Cell* 4(6):841–852.
62. Atkin JD, et al. (2006) Induction of the unfolded protein response in familial amyotrophic lateral sclerosis and association of protein-disulfide isomerase with superoxide dismutase 1. *J Biol Chem* 281(40):30152–30165.
63. Kikuchi H, et al. (2006) Spinal cord endoplasmic reticulum stress associated with a microsomal accumulation of mutant superoxide dismutase-1 in an ALS model. *Proc Natl Acad Sci USA* 103(15):6025–6030.
64. Tobisawa S, et al. (2003) Mutant SOD1 linked to familial amyotrophic lateral sclerosis, but not wild-type SOD1, induces ER stress in COS7 cells and transgenic mice. *Biochem Biophys Res Commun* 303(2):496–503.
65. Wate R, et al. (2005) Expression of an endoplasmic reticulum-resident chaperone, glucose-regulated stress protein 78, in the spinal cord of a mouse model of amyotrophic lateral sclerosis. *Acta Neuropathol* 110(6):557–562.
66. Vlug AS, et al. (2005) ATF3 expression precedes death of spinal motoneurons in amyotrophic lateral sclerosis-SOD1 transgenic mice and correlates with c-Jun phosphorylation, CHOP expression, somato-dendritic ubiquitination and Golgi fragmentation. *Eur J Neurosci* 22(8):1881–1894.
67. DuRose JB, Tam AB, Niwa M (2006) Intrinsic capacities of molecular sensors of the unfolded protein response to sense alternate forms of endoplasmic reticulum stress. *Mol Biol Cell* 17(7):3095–3107.
68. Saxena S, Cabuy E, Caroni P (2009) A role for motoneuron subtype-selective ER stress in disease manifestations of FALS mice. *Nat Neurosci* 12(5):627–636.
69. Kiskinis E, et al. (2014) Pathways disrupted in human ALS motor neurons identified through genetic correction of mutant SOD1. *Cell Stem Cell* 14(6):781–795.
70. Nishitoh H, et al. (2008) ALS-linked mutant SOD1 induces ER stress- and ASK1-dependent motor neuron death by targeting Derlin-1. *Genes Dev* 22(11):1451–1464.
71. Vande Velde C, Miller TM, Cashman NR, Cleveland DW (2008) Selective association of misfolded ALS-linked mutant SOD1 with the cytoplasmic face of mitochondria. *Proc Natl Acad Sci USA* 105(10):4022–4027.
72. Liu J, et al. (2004) Toxicity of familial ALS-linked SOD1 mutants from selective recruitment to spinal mitochondria. *Neuron* 43(1):5–17.
73. Israelson A, et al. (2010) Misfolded mutant SOD1 directly inhibits VDAC1 conductance in a mouse model of inherited ALS. *Neuron* 67(4):575–587.
74. Homma K, et al. (2013) SOD1 as a molecular switch for initiating the homeostatic ER stress response under zinc deficiency. *Mol Cell* 52(1):75–86.
75. Israelson A, et al. (2015) Macrophage migration inhibitory factor as a chaperone inhibiting accumulation of misfolded SOD1. *Neuron* 86(1):218–232.
76. Lim L, Lee X, Song J (2015) Mechanism for transforming cytosolic SOD1 into integral membrane proteins of organelles by ALS-causing mutations. *Biochim Biophys Acta* 1848(1 Pt A):1–7.
77. Matus S, Lopez E, Valenzuela V, Nassif M, Hetz C (2013) Functional contribution of the transcription factor ATF4 to the pathogenesis of amyotrophic lateral sclerosis. *PLoS One* 8(7):e66672.
78. Hetz C, et al. (2009) XBP-1 deficiency in the nervous system protects against amyotrophic lateral sclerosis by increasing autophagy. *Genes Dev* 23(19):2294–2306.
79. Wang L, Popko B, Roos RP (2011) The unfolded protein response in familial amyotrophic lateral sclerosis. *Hum Mol Genet* 20(5):1008–1015.
80. Kim HJ, et al. (2014) Therapeutic modulation of eIF2α phosphorylation rescues TDP-43 toxicity in amyotrophic lateral sclerosis disease models. *Nat Genet* 46(2):152–160.
81. Trapnell C, Pachter L, Salzberg SL (2009) TopHat: Discovering splice junctions with RNA-Seq. *Bioinformatics* 25(9):1105–1111.
82. Mortazavi A, Williams BA, McCue K, Schaeffer L, Wold B (2008) Mapping and quantifying mammalian transcriptomes by RNA-Seq. *Nat Methods* 5(7):621–628.
83. Trapnell C, et al. (2010) Transcript assembly and quantification by RNA-Seq reveals unannotated transcripts and isoform switching during cell differentiation. *Nat Biotechnol* 28(5):511–515.